CARBON 48 (2010) 4162–4169

available at www.sciencedirect.com

ScienceDirect

journal homepage: www.elsevier.com/locate/carbon

Comparison of the Dubinin–Radushkevich and Quenched Solid Density Functional Theory approaches for the characterisation of narrow microporosity in activated carbons obtained by chemical activation with KOH or NaOH of Kraft and hydrolytic lignins

P.J.M. Carrott *, *M.M.L. Ribeiro Carrott*, *Suhas*

Centro de Química de Évora and Departamento de Química, Universidade de Évora, Colégio Luís António Verney, 7000-671 Évora, Portugal

ARTICLE INFO

Article history:
Received 10 April 2010
Accepted 21 July 2010
Available online 25 July 2010

ABSTRACT

The classical DR method and the Quenched Solid Density Functional Theory (QSDFT) approach have been used to analyse N_2 at 77 K isotherms determined on activated carbons prepared by alkaline chemical activation of different lignins. The QSDFT pore size distributions are bimodal with a narrow peak below 1 nm and a broad peak from 1 to 2.5–3.5 nm. Deconvolution allows estimation of the volumes and widths of the narrow micropores. These are lower than estimated by the DR analysis as this does not separate micropore and non-micropore adsorption. On the basis of the QSDFT analysis, the optimum conditions for obtaining materials with a high volume of narrow micropores were activation temperatures of 550–650 °C, hydroxide/lignin ratio of 1 and dwell time at the maximum activation temperature of 30 min. KOH was preferable to NaOH as it requires lower temperatures and results in materials with higher narrow micropore volumes. The "best" material obtained, prepared with KOH at 550 °C, had mean micropore width of 0.7 nm and micropore volume of 0.37 $cm^3\ g^{-1}$ which compares very favourably with molecular sieve carbons prepared from synthetic polymers. Furthermore, this material was obtained with an activation yield of 32.9%, which is quite high for alkaline chemical activation.

1. Introduction

The first works dealing with the preparation of activated carbons from lignin were published about 30 years ago and subsequently there has been a number of new studies [1]. Most of the work so far published has dealt with the characterisation of porosity and reactivity of activated carbons prepared from raw [2–18], demineralised [18–23] and alkali metal impregnated [18,19] Kraft [5–12,18–23] and other lignins [2,4,12–17] by physical activation with CO_2 [4–6,12,18–20] and water vapour [12] and chemical activation with $ZnCl_2$ [8,15], H_3PO_4 [9–11,13–15,23] and alkaline hydroxides or carbonates [2,3,15–17,21,22]. In much of this published work attention has been focussed on obtaining materials with very high surface areas and total pore volumes, and values of BET surface area well in excess of 2000 $m^2\ g^{-1}$, corresponding to total pore volumes greater than 1 $cm^3\ g^{-1}$, have been reported [2,21,22]. In general, such high BET areas are only obtained when the pore size is comparatively large, and the pore size distribution extends into the range of small mesopores. However, there are certain applications, such as adsorption of VOCs (volatile organic compounds) from the gas phase [24,25] or phenolic

* *Corresponding author:* Fax: +351 266745303.
E-mail address: peter@uevora.pt (P.J.M. Carrott).
0008-6223/$ - see front matter
doi:10.1016/j.carbon.2010.07.031

pollutants from the aqueous phase [26,27], where a high volume of narrow micropores, less than 1 nm in width, is advantageous due to the enhanced heat of adsorption which occurs in narrow micropores. The characterisation of this porosity is dependent on the analysis of adsorption isotherms, principally of N_2 at 77 K.

The classical methods of isotherm analysis, such as the α_s, *t*-plot and DR methods have played an extremely important role in directing microporous carbon materials development over the last 50 years, and they are still extensively used. However, they tend to provide an overview of the pore structure. Methods based on molecular simulation or density functional theory, available since 1989 [28,29], have the potential to provide the more precise information which is needed for modern tailored materials development. A number of theoretical studies have been published in which the Grand Canonical Monte Carlo method has been used to simulate adsorption isotherms in slit-shaped carbon pores and these were subsequently analysed by the DR method [30–32]. These studies were successful in highlighting some of the difficulties associated with the interpretation of the results of analysing adsorption isotherms by the DR method. Of particular relevance here is the possibility of estimating a mean micropore size or of calculating a pore size distribution (PSD). It is well known that the Dubinin theory does not apply to single pore isotherms and it has recently been shown by Do, Nicholson and Do that this remains true even when defects are introduced into the pore wall surfaces [30]. Furthermore, according to this study "for a given characteristic energy, the Dubinin equation corresponds to a solid with a specific pore size distribution". On the other hand, Ohba and Kaneko demonstrated that "simulated DR plots with different half-widths of PSD having Gaussian and Gaussian-like distributions of average pore width 1.2 nm were almost the same as each other" over the usual range of linearity of DR plots (approximately 10^{-4} to 10^{-2} p^o) [31]. Hence, both studies question the feasibility of obtaining reliable pore size distributions within the context of the Dubinin theory, particularly when the PSD is very narrow or when it extends into the region of wider micropores.

Molecular simulation or density functional theory allow single pore isotherms to be calculated and on the basis of these, calculated for pores of different widths, it is possible to estimate pore size distributions. Most commercial adsorption equipment manufacturers now provide suitable software based on molecular simulation or the so-called Non-Local Density Functional Theory (NLDFT) [33]. In the case of carbons the pores are usually assumed to be infinite parallel sided slits with ideal graphitic surfaces and the theoretical adsorption isotherms in these pores exhibit steps associated with layering transitions. Hence the computational procedure for calculating the PSD from an experimental isotherm will interpret increase in adsorption at the corresponding values of p/p^o as a layering transition and as a result the calculated PSDs will tend to exhibit false minima at the corresponding values of pore width (typically ~1 and ~2 nm) [34,35]. A solution to this problem is to minimize the layering transitions in the theoretical isotherms by introducing heterogeneity into the pore model and a number of approaches have been proposed. For instance, Jagiello and Olivier have recently shown that a pore model based on finite parallel sided slits leads to better agreement between theory and experiment [36]. Do and Do introduced heterogeneity by selectively removing carbon atoms or groups of carbon atoms from the top surface layer [37]. Variability in pore wall thickness [38–40] and other approaches [41,42] have also been tested. Most of these new procedures are not yet available commercially. One exception to this, originally developed by Ravikovitch and Neimark, is referred to as Quenched Solid Density Functional Theory (QSDFT) [35,43].

In the QSDFT method the solid surface is described by a linear density profile of atoms instead of the more usual step function. In this way the surface geometrical heterogeneity can be characterised by a single roughness parameter, δ, which represents the half width of the density ramp. By adjusting δ and the fluid–solid interaction parameters the model can be adapted for a given type of material by fitting to an experimental adsorption isotherm on a well-characterised reference surface. In Ref. [35] Cabot BP-280, a partially graphitised carbon black, is used as the reference surface and the roughness parameter is $\delta \sim 0.13$ nm. The layering transitions are still present but are significantly reduced, and it has been shown, for instance, that pore size distributions of microporous mesoporous carbon aerogels show pronounced minima at ~1 and ~2 nm when using the NLDFT method but do not when QSDFT is used [44]. Additional examples for other types of microporous carbon are given in the original paper [35].

The objective of the work reported here was to assess the applicability of QSDFT, and compare its predictions with those of the DR method, for characterising the narrow microporosity of a different type of activated carbon to that used in Ref. [44], namely activated carbon prepared from lignin. Dry impregnation with NaOH and KOH was chosen as the activation method as other work has shown that this procedure is particularly effective with lignin precursors [2,16,21,22].

2. Experimental

2.1. Materials and methods

The Kraft and hydrolytic lignins used here were the same as those used in our previous work [12,19] where details can be found. For the production of the activated carbons the lignin was first mixed with dry NaOH or KOH in the desired ratio (1:0.5, 1:1, 1:2, 1:3 or 1:4) and then about 5 g of the mixture were placed in a ceramic boat and positioned in the central constant temperature zone of a conventional horizontal tubular furnace. Activation was carried out by heating to the desired temperature (550, 650, 750 or 850 °C) at a rate of 8 °C min^{-1} under a constant N_2 flow of 85 cm^3 min^{-1} and maintaining for 30 or 90 min. After allowing to cool to below 50 °C the product was removed from the furnace, washed with distilled water until constant pH, filtered and dried at 110 °C overnight before storing in sealed sample flasks. The yield, Y, of the samples was calculated from

$$Y = 100w/w_o \quad (1)$$

where w_o is the weight of lignin and w is the final weight of activated carbon after removal of the impregnant.

2.2. Characterisation

Characterisation of the Kraft and hydrolytic lignins by XRD, thermogravimetric analysis and FTIR, as well as elemental analyses of C, H, N, S and O, and humidity and ash determinations according to ASTM and ISO standards, have been described previously [12,18]. N_2 isotherms at 77 K were determined using automated adsorption equipment from CE Instruments or Quantachrome, using helium (for dead space calibration) and nitrogen of 99.999% purity supplied, respectively, by Linde and Air Liquide. Prior to the adsorption measurements all samples were outgassed for 4 h at 300 °C. The N_2 isotherms were analysed by means of the α_s method using published standard data in order to obtain the total pore volume v_s [45]. They were also analysed by means of the DR equation in order to obtain the DR pore volume, v_o, and the corresponding estimate of apparent mean pore width, L_o, from the relationship [46]:

$$L_0 = 10.8/(E_o - 11.4) \quad (2)$$

where E_o is the characteristic energy obtained by application of the DR equation. The liquid density of N_2 was taken as 0.808 g cm^{-3} and the affinity coefficient as $\beta = 0.34$ [47]. In addition, the Quantachrome AS1Win™ version 2.01 software package was used to calculate pore size distributions assuming slit-shaped pores and using the quenched solid DFT (QSDFT) model. Deconvolution of the pore size distributions was carried out using the program Igor Pro© version 6.1.2.1.

3. Results and discussion

3.1. Classical analysis of N_2 adsorption isotherms

Representative N_2 adsorption isotherms are shown in Fig. 1. The isotherms presented Type I character in all cases indicating that the samples were predominantly microporous. However, with increase in the activation temperature, activation time or impregnation ratio, the isotherms became more rounded and for some samples a Type H4 hysteresis loop appeared. These features indicate a broadening of the pore size distribution into the small mesopore range as the intensity of the activation increased. In general, it was found that the isotherms determined on KOH activated samples were more rounded than those determined on corresponding NaOH activated samples, indicating greater widening of the pore size in the former case.

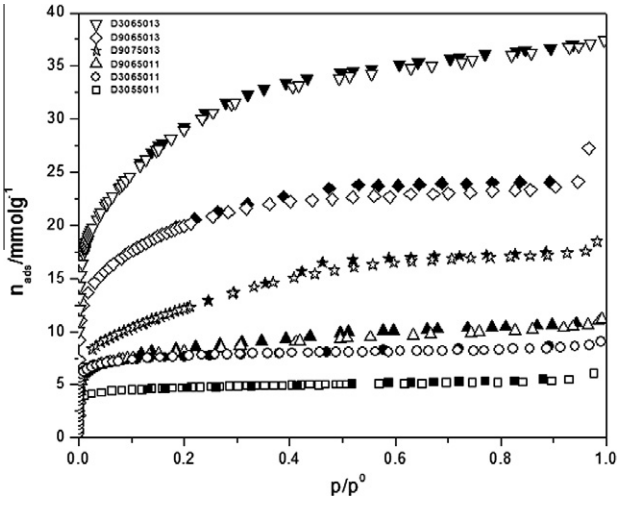

Fig. 1 – Representative N_2 at 77 K adsorption isotherms determined on NaOH activated hydrolytic lignin. Open symbols: adsorption, closed symbols: desorption. Nomenclature = D*tt*T*TT*1*r* where *tt* is dwell time (min) at temperature *TTT* (°C) and *r* is hydroxide/lignin ratio.

The results of the analysis of the isotherms by the BET, α_s and DR methods are given in Tables 1 and 2. It can be seen that under appropriate conditions high BET surface areas (>2000 m^2 g^{-1}) and total pore volumes (>1.0 cm^3 g^{-1}) were obtained, although in most cases these were associated with comparatively high values of L_o (>1.5 nm). It is particularly notable that the high BET surface areas and total pore volumes were more readily obtained by KOH activation. For these samples, the highest value of BET surface area obtained was 2788 m^2 g^{-1} for a sample of hydrolytic lignin with $r = 3$ and activated for 90 min at 750 °C. On the other hand, the highest total pore volume (1.36 cm^3 g^{-1}) was obtained for a sample of Kraft lignin with $r = 4$ and activated for 30 min at 750 °C. A very similar result (1.34 cm^3 g^{-1}) was obtained with the same Kraft lignin and activation temperature but with $r = 3$ and activated for 90 min. The reason for this difference between the Kraft and hydrolytic lignins is that the latter not only gives lower pore volumes, but it also gives lower L_o values, and hence the BET area, which is sensitive to both pore volume and the distribution of micropore sizes, is higher.

A more detailed analysis of the data in the tables confirms that they are in overall agreement with previous work using Kraft lignin from the same source as ours [21]. Thus, in general, KOH gives higher BET areas, total pore volumes and L_o values, than NaOH and, for obtaining high BET area and total pore volume, the optimum activation temperature is around 650–750 °C, the impregnation ratio should be 3–4 and relatively lengthy activation times should be used. On the other hand, the values of BET surface area and total pore volume which we obtained appear to be very slightly lower than those reported in Ref. [21]. For example, these authors obtained materials with BET areas of approximately 3000 ± 100 m^2 g^{-1} under conditions similar to our product with BET area of 2788 m^2 g^{-1}. This difference may be due to the fact that the previous authors demineralised the lignin before use, whereas we decided not to do this in this work. This was because, on the one hand, the ash content will be removed during the final washing of the activated carbon and, on the other, we wanted to determine if the presence of ash (mainly sodium carbonate sulfate [12,19]) had a significant influence on the properties of the materials obtained by chemical activation. It has already been shown that demineralisation is essential before physical activation of Kraft lignin [12], but its effect during alkaline chemical activation does not appear to have been clarified yet. Comparison of the present results with those in Ref. [21] suggests that omitting the pre-activation demineralisation has only a relatively small effect on the properties of the materials obtained.

Table 1 – Results of BET, α_s, DR and QSDFT analyses of the textural characteristics of activated carbons obtained from Kraft and hydrolytic lignins by chemical activation using NaOH.[a].

Time (min)	r	T (°C)	A_{BET} ($m^2\ g^{-1}$)	v_s ($cm^3\ g^{-1}$)	v_o ($cm^3\ g^{-1}$)	v_1 ($cm^3\ g^{-1}$)	L_o (nm)	d_1 (nm)	Y (%)
Kraft lignin									
30	1	550	714	0.26	0.22	0.13	1.40	0.71	29.1
30	1	650	1140	0.40	0.35	0.23	1.15	0.74	24.6
30	1	750	1389	0.55	0.41	0.27	1.27	0.67	14.9
30	1	850	1209	0.56	0.37	0.24	1.37	0.77	7.3
30	0.5	750	990	0.37	0.31	0.28	1.02	0.77	21.4
30	2	750	1936	0.82	0.52	0.32	1.53	0.76	7.6
30	3	750	2214	1.05	0.59	0.33	1.76	0.84	3.1
90	1	750	1041	0.43	0.32	0.24	1.46	0.81	6.4
90	3	750	1218	0.66	0.36	[b]	1.87	[b]	1.3
Hydrolytic lignin									
30	1	550	398	0.14	0.13	0.07	0.89	0.66	35.5
30	1	650	654	0.22	0.21	0.20	0.95	0.60	29.5
30	1	750	586	0.26	0.20	0.15	1.12	0.75	19.5
30	1	850	323	0.12	0.11	[b]	1.92	[b]	8.2
30	3	650	2227	0.95	0.59	0.19	1.12	0.60	10.8
90	1	650	670	0.26	0.20	0.09	0.84	0.60	16.9
90	1	750	637	0.23	0.20	0.16	1.17	0.76	13.4
90	3	650	1609	0.63	0.47	0.26	1.53	0.78	5.2
90	3	750	982	0.47	0.28	0.16	1.83	0.78	4.5

[a] t = dwell time at activation temperature; r = ratio hydroxide/lignin; T = activation temperature; A_{BET} = apparent surface area obtained by BET method; v_s = total pore volume obtained by α_s method; v_o and L_o = micropore volume and mean pore width from DR plot; v_1 and d_1 = micropore volume and mean pore width from first peak of QSDFT pore size distribution.
[b] insufficient points at very low p/p^o for pore size distribution calculation.

Table 2 – Results of BET, α_s, DR and QSDFT analyses of the textural characteristics of activated carbons obtained from Kraft and hydrolytic lignins by chemical activation using KOH.[a].

Time (min)	r	T (°C)	A_{BET} (m^2g^{-1})	v_s (cm^3g^{-1})	v_o (cm^3g^{-1})	v_1 (cm^3g^{-1})	L_o (nm)	d_1 (nm)	Y (%)
Kraft lignin									
30	1	550	1186	0.39	0.40	0.37	0.87	0.70	32.9
30	1	650	1829	0.66	0.55	0.40	1.20	0.76	25.7
30	1	750	1130	0.53	0.35	0.29	1.92	0.80	21.5
30	1	850	978	0.46	0.30	0.16	1.80	0.80	6.4
30	3	650	2285	1.02	0.72	0.37	2.12	0.84	22.6
30	4	650	2460	1.16	0.57	[b]	1.12	[b]	17.1
30	4	750	2452	1.36	0.76	0.40	2.40	0.94	9.8
90	1	650	2026	0.80	0.58	[b]	1.46	[b]	20.5
90	1	750	1868	0.70	0.60	0.24	1.61	0.76	17.7
90	3	650	2444	1.08	0.73	0.41	1.87	0.84	19.2
90	3	750	2647	1.34	0.73	0.41	2.23	0.90	9.1
Hydrolytic lignin									
30	1	650	1496	0.50	0.47	0.37	0.98	0.71	23.3
30	1	750	1682	0.66	0.51	0.36	1.32	0.77	17.1
30	1	850	1363	0.54	0.43	0.40	1.46	0.96	5.8
30	4	750	2212	1.04	0.61	[b]	1.65	[b]	15.5
90	1	750	1530	0.55	0.48	0.51	1.39	0.80	11.5
90	3	750	2788	1.18	0.81	0.36	1.97	0.83	8.2

[a] t = dwell time at activation temperature; r = ratio hydroxide/lignin; T = activation temperature; A_{BET} = apparent surface area obtained by BET method; v_s = total pore volume obtained by α_s method; v_o and L_o = micropore volume and mean pore width from DR plot; v_1 and d_1 = micropore volume and mean pore width from first peak of QSDFT pore size distribution.
[b] Insufficient points at very low p/p^o for pore size distribution calculation.

3.2. *Quenched Solid Density Functional Theory analysis of N_2 adsorption isotherms*

Representative N_2 adsorption isotherms with p/p^o on a logarithmic scale are shown in Fig. 2. Additional examples are also included in the Supplementary Information. The solid and dotted lines on the figures are the fits of the QSDFT and NLDFT models, respectively, and it is clear that the QSDFT model gives better fits to the experimental data. For example, for the Kraft lignin sample in Fig. 2 the fitting errors are 0.26%

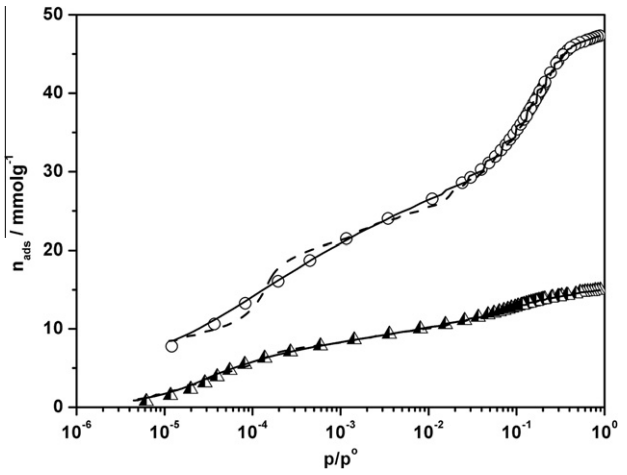

Fig. 2 – Comparison of fits to the experimental N_2 isotherms measured at 77 K. Open circles = hydrolytic lignin activated with KOH/lignin ratio 3 at 750 °C for 90 min. Half-filled triangles = Kraft lignin activated with NaOH/lignin ratio 1 at 650 °C for 30 min. Solid lines = QSDFT fit. Dashed lines = NLDFT fit. For clarity, the top curve has been shifted upwards by 5 mmol g^{-1}.

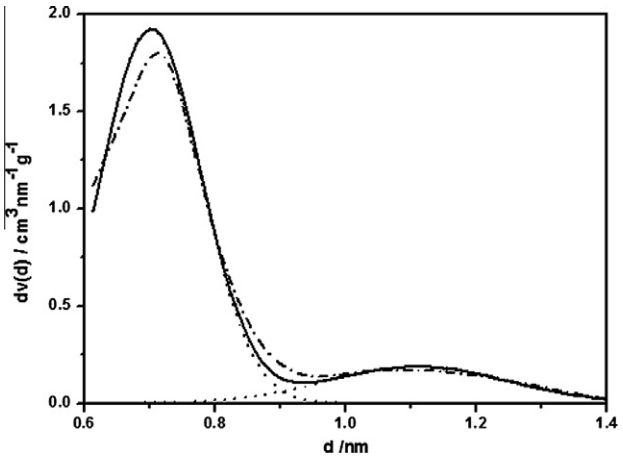

Fig. 4 – Deconvolution of QSDFT pore size distribution of activated carbon prepared from Kraft lignin with KOH/lignin ratio 1 and activated at 550 °C for 30 min. Dot–dash line = QSDFT pore size distribution; dotted lines = fitted Gaussian peaks; solid line = sum of Gaussian peaks.

and 0.98%, respectively, for QSDFT and NLDFT. Representative QSDFT pore size distributions are shown in Figs. 3 and 4. Both QSDFT and NLDFT pore size distributions for all the samples in Figs. 2–4 can be found in the Supplementary Information. The most evident feature of the QSDFT pore size distributions is that they appear to be bimodal. The first peak of each pore size distribution curve is narrower having, in most cases, a peak width at half-height between 0.1 and 0.5 nm and a maximum which occurs at a pore width of between 0.6 and 0.9 nm. The second peak is only very significant with the more intensely activated samples and generally occurs over a range extending from about 1 nm up to 2.5–3.5 nm, depending on the sample. It is notable that with increase in the upper limit the second peak becomes very flat-topped. This was particularly clear with the samples with the highest total pore volumes, namely Kraft lignin activated with KOH at 750 °C with $r = 4$ and $t = 30$ min and with $r = 3$ and $t = 90$ min. On the other hand, the sample with the highest BET surface area, hydrolytic lignin activated with KOH at 750 °C with $r = 3$ and $t = 90$ min, gives a more symmetrical second peak with a lower upper limit of pore size. Hence, the QSDFT analysis indicates that the hydrolytic lignin has a higher BET surface area, even though the total pore volume is lower, because a higher proportion of the porosity is present in smaller pores. This is in agreement with the remark made in the previous section based on the classical analysis of the isotherm data.

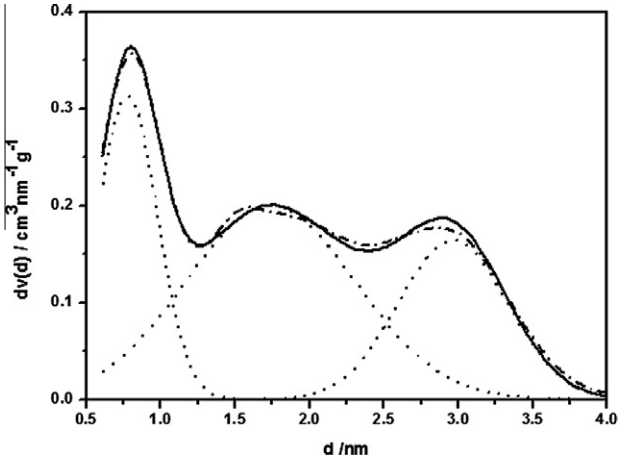

Fig. 3 – Deconvolution of QSDFT pore size distribution of activated carbon prepared from hydrolytic lignin with NaOH/lignin ratio 3 and activated at 750 °C for 90 min. Dot–dash line = QSDFT pore size distribution; dotted lines = fitted Gaussian peaks; solid line = sum of Gaussian peaks.

The first peak occurs over the range of pore sizes where there is an enhancement in the heat of adsorption and this porosity will be more important during the adsorption of organic vapours at low partial pressures or of small organic solutes, such as phenols, present in low concentrations. As this peak is fairly well separated from the second peak, an estimate of its area, which is equal to the corresponding micropore volume, can be obtained by deconvoluting the pore size distribution. We have carried this out by fitting 2 or 3 gaussian functions to each pore size distribution. As can be seen from the representative examples in Figs. 3 and 4 the fits were very good. For some samples there was a small overlap between the first fitted peak and the second (Fig. 3 is an extreme case) and hence the estimated micropore volume will be a lower bound. For the first peak, the positions (d_1) and corresponding pore volumes (v_1) are given in Tables 1 and 2.

It can be seen from the tables that the values of v_1 and d_1, obtained from each first peak, are lower than the estimates of micropore volume, v_o, and mean pore width, L_o, obtained by the classical DR analysis. The latter was carried out using the raw isotherm data and hence the ordinate values of the DR plots include the adsorption on the walls of wider pores and on external surface [48], whereas this adsorption is (in

principle) separated out during a DFT pore size distribution analysis. As previously shown [49], the lack of a correction for pore wall and external surface adsorption leads to a significant increase in the derived values of v_o and L_o. It has also been shown previously that when applied to low temperature N_2 isotherm data determined on exclusively narrow microporous activated carbons, Eq. (2) tends to overestimate the micropore size by about 0.2 nm [50]. Hence, at least in qualitative terms, the difference between corresponding values of v_o and v_1, on the one hand, and L_o and d_1, on the other, are not surprising.

A clearer picture of the differences can be seen from Figs. 5 and 6, where v_o and L_o are plotted as a function of v_1 and d_1. It can be seen that for the majority of samples the DR v_o values are between 1 and 2 times greater than the QSDFT v_1 values. The DR L_o values are also between 1 and 2 times greater than the QSDFT d_1 values for d_1 less than about 0.75 nm, but bigger differences are found for larger pore sizes. It is interesting to note that 0.75 nm is close to twice the diameter of an N_2 molecule and hence the limit for enhancement of the heat of adsorption of N_2 in slit-shaped carbon micropores [51]. Hence, the results in Figs. 5 and 6 confirm that the DR estimate of micropore volume includes not only the narrow micropores (often called ultramicropores or primary micropores [52–54]), where the heat of adsorption is enhanced, but also a range of wider micropores whose extent varies from one sample to another.

From the results in the tables and from Fig. 5 it can be seen that, in general, for each type of lignin precursor, higher v_1 micropore volumes are found with the KOH activated samples. For NaOH activation, higher micropore volumes are generally given by the Kraft lignin derived samples while, for KOH activation it is not possible to draw a conclusion on the basis of the data available. Similarly, it is not possible to draw firm conclusions about the relationship between d_1 and lignin type or activating agent from Fig. 6.

One of the overall objectives of the work was to identify the most suitable conditions for obtaining materials with a high volume of narrow micropores. The results in Tables 1 and 2 show that these are obtained under mild conditions of activation. If we just consider samples with $d_1 < 0.75$ nm, then 10 of the 30 samples for which it was possible to calculate pore size distributions would be satisfactory. Eight of these were obtained with 30 min activation time and hydroxide/lignin ratio of 1. With NaOH as activation agent temperatures of 550, 650 or 750 °C were used, while with KOH as activating agent it was only possible to obtain two satisfactory samples, one at 550 °C from Kraft lignin and one at 650 °C from hydrolytic lignin. For each of the four hydroxide/lignin systems the samples with the lowest d_1 values were obtained under time/ratio/temperature conditions of 30 min/r1/750 °C (NaOH/Kraft), 30 min/r1/650 °C (NaOH/hydrolytic), 30 min/r1/550 °C (KOH/Kraft) and 30 min/r1/650 °C (KOH/hydrolytic). These conditions (with the exception of temperature, where 650–750 °C is recommended) are the opposite of those for maximising the BET surface area and the total pore volume of lignin derived activated carbons.

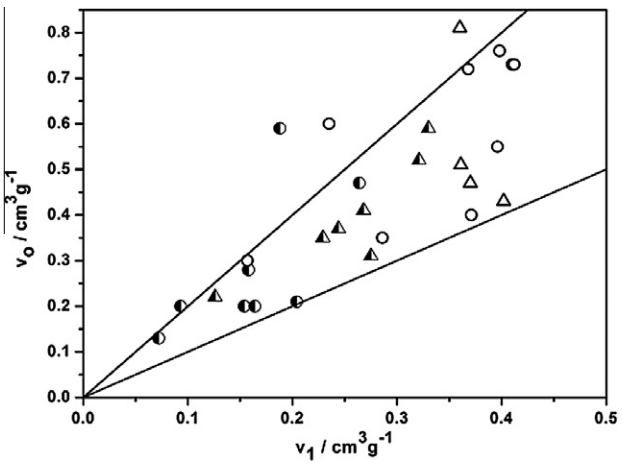

Fig. 5 – Relationship between micropore volumes v_o and v_1 estimated by the DR and QSDFT analyses. Half-filled symbols = NaOH; empty symbols = KOH; triangles = Kraft; circles = hydrolytic. Solid lines have slopes of 1 and 2.

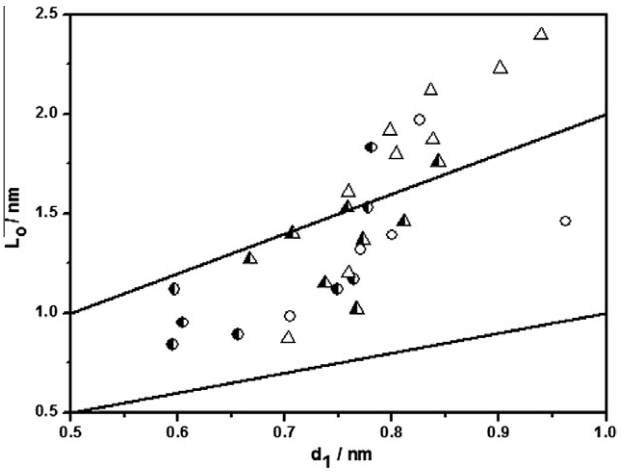

Fig. 6 – Relationship between mean pore widths L_o and d_1 estimated by the DR and QSDFT analyses. Half-filled symbols = NaOH; empty symbols = KOH; triangles = Kraft; circles = hydrolytic. Solid lines have slopes of 1 and 2 and intercept 0.

3.3. *Activation yields*

An important aspect of any activation process is the amount of precursor which is converted into final product. The overall activation yields for the samples prepared in this work are given in the final column of Tables 1 and 2 and vary between 1.3% and 35.5%. As expected, the yields decrease as the activation time, activation temperature or hydroxide/lignin ratio increase. Under similar conditions the yields obtained with the hydrolytic lignin are up to about 5% higher than those obtained with the Kraft lignin. The yields obtained using KOH are generally higher, by a few %, during activation of the Kraft lignin, but lower during activation of the hydrolytic lignin. There is no direct relationship between yield and surface area of the products. However, very high surface areas (>2500 $m^2 g^{-1}$) are only obtained with low yields <10%, and high surface areas (2000–2500 $m^2 g^{-1}$) with yields in the range 10–20% in most cases.

For the 10 microporous samples with $d_1 < 0.75$ nm the yields vary from 14.9% to 35.5% and, for each of the four hydroxide/lignin systems, the samples with the lowest d_1 values referred to in the previous section, are obtained with yields from 14.9% to 32.9%. Overall, KOH activation of Kraft or hydrolytic lignin at 550–650 °C with $r = 1$ and $t = 30$ min gives the best combination of high yield, high micropore volume and low pore size. The main advantage of KOH over NaOH is principally in relation to narrow micropore volumes, v_1, about 1.4 to two times higher.

4. Conclusions

The results presented indicate that, in contrast to physical activation with CO_2 [12], demineralisation of lignin has a relatively small influence on the properties of activated carbons prepared by alkaline chemical activation. As a result, materials with similar properties are obtained from impure or demineralised [21] Kraft or pure hydrolytic lignin precursors.

Low temperature N_2 isotherms determined on activated carbons prepared from the lignin precursors can be analysed by applying the classical α_s and DR methods. However, useful complementary information, particularly in relation to the narrow microporosity of the materials, is provided by use of the Quenched Solid DFT model [35,43] for calculation of the pore size distribution. This was successfully applied here and showed that pore size distributions of lignin based activated carbons are bimodal. A narrow peak is always found at pore widths below 1 nm and a broad peak is generally found over the range from 1 nm to 2.5 or 3.5 nm, depending on the sample. Deconvolution of the pore size distributions allows the volumes and corresponding mean pore widths of the narrow micropores to be estimated. The values obtained are lower than those estimated by the classical DR analysis which is due, at least in part, to the lack of a correction for mesopore and external surface adsorption in the DR method [49].

On the basis of the results of the QSDFT analysis the optimum conditions for obtaining materials with a high volume of narrow micropores can be identified. The best results were obtained using activation temperatures of about 550–650 °C, hydroxide/lignin ratio of 1 and dwell time at the maximum activation temperature of 30 min. KOH was found to be preferable to NaOH as it requires lower activation temperatures and results in materials with higher narrow micropore volumes. The "best" material obtained, prepared with KOH at 550 °C, had a mean micropore width of 0.7 nm and a micropore volume of 0.37 $cm^3\ g^{-1}$ which compares very favourably with molecular sieve carbons prepared from synthetic polymers [55,56]. Furthermore, this material was obtained with an activation yield of 32.9%, which is quite high for alkaline chemical activation.

Acknowledgements

This work was supported by the Fundacão para a Ciência e a Tecnologia (Plurianual Finance Project Centro de Química de Évora (619) and post-doctoral Grant SFRH/BPD/20535/2004) with national and European community (FEDER) funds and by the Lignocarb Project funded by the European Commission (Project ALFA-II-0412-FAFI). The authors thank Dr. V. Fierro for providing the Kraft lignin.

Appendix A. Supplementary data

Supplementary data associated with this article can be found, in the online version, at doi:10.1016/j.carbon.2010.07.031.

REFERENCES

[1] Suhas, Carrott PJM, Carrott MMLR. Lignin – from natural adsorbent to activated carbon: a review. Bioresour Technol 2007;98(12):2301–12.
[2] Zou Y, Han BX. Preparation of activated carbons from Chinese coal and hydrolysis lignin. Adsorpt Sci Technol 2001;19:59–72.
[3] Khezami L, Chetouani A, Taouk B, Capart R. Production and characterisation of activated carbon from wood components in powder: cellulose, lignin, xylan. Powder Technol 2005;157:48–56.
[4] Baklanova ON, Plaksin GV, Drozdov VA, Duplyakin VK, Chesnokov NV, Kuznetsov BN. Preparation of microporous sorbents from cedar nutshells and hydrolytic lignin. Carbon 2003;41:1793–800.
[5] Rodríguez-Mirasol J, Cordero T, Rodríguez JJ. Activated carbons from CO_2 partial gasification of eucalyptus Kraft lignin. Energy Fuel 1993;7:133–8.
[6] Rodríguez-Mirasol J, Cordero T, Rodríguez JJ. CO_2-reactivity of eucalyptus Kraft lignin chars. Carbon 1993;31:53–61.
[7] Sharma RK, Wooten JB, Baliga VL, Lin XH, Chan WG, Hajaligol MR. Characterization of chars from pyrolysis of lignin. Fuel 2004;83:1469–82.
[8] González-Serrano E, Cordero T, Rodríguez-Mirasol J, Rodríguez JJ. Development of porosity upon chemical activation of Kraft lignin with $ZnCl_2$. Ind Eng Chem Res 1997;36:4832–8.
[9] Fierro V, Torné-Fernández V, Montané D, Celzard A. Study of the decomposition of Kraft lignin impregnated with orthophosphoric acid. Thermochim Acta 2005;433(1–2):142–8.
[10] González-Serrano E, Cordero T, Rodríguez-Mirasol J, Cotoruelo L, Rodríguez JJ. Removal of water pollutants with activated carbons prepared from H_3PO_4 activation of lignin from Kraft black liquors. Water Res 2004;38:3043–50.
[11] Guo Y, Rockstraw D. Physical and chemical properties of carbons synthesized from xylan, cellulose, and Kraft lignin by H_3PO_4 activation. Carbon 2006;44(8):1464–75.
[12] Carrott PJM, Suhas, Carrott MMLR, Guerrero CI, Delgado LA. Reactivity and porosity development during pyrolysis and physical activation in CO_2 or steam of Kraft and hydrolytic lignins. J Anal Appl Pyrolysis 2008;82:264–71.
[13] Kriaa A, Hamdi N, Srasra E. Removal of Cu (II) from water pollutant with Tunisian activated lignin prepared by phosphoric acid activation. Desalination 2010;250(1):179–87.
[14] Mussatto S, Fernandes M, Rocha G, Órfão J, Teixeira J, Roberto I. Production, characterization and application of activated carbon from Brewer's spent grain lignin. Bioresour Technol 2010;101(7):2450–7.
[15] Hayashi J, Kazehaya A, Muroyama K, Watkinson A. Preparation of activated carbon from lignin by chemical activation. Carbon 2000;38(13):1873–8.
[16] Babeł K, Jurewicz K. KOH activated lignin based nanostructured carbon exhibiting high hydrogen electrosorption. Carbon 2008;46(14):1948–56.
[17] Sun Y, Wei J, Wang Y, Yang G, Zhang J. Production of activated carbon by K_2CO_3 activation treatment of cornstalk lignin and

its performance in removing phenol and subsequent bioregeneration. Environ Technol 2010;31(1):53–61.
[18] Carrott PJM, Carrott MMLR, Suhas, Mourão PAM, Guerrero CI, Delgado LA. Reactivity of cork and lignin for the production of activated carbons. Mater Sci Forum 2008;587–588:618–22.
[19] Suhas, Carrott PJM, Carrott MMLR. Using alkali metals to control reactivity and porosity during physical activation of demineralised Kraft lignin. Carbon 2009;47:1012–7.
[20] Cotoruelo L, Marqués M, Díaz F, Rodríguez-Mirasol J, Cordero T, Rodríguez J. Activated carbons from lignin: their application in liquid phase adsorption. Sep Sci Technol 2007;42(15):3363–89.
[21] Fierro V, Torné-Fernández V, Celzard A. Methodical study of the chemical activation of Kraft lignin with KOH and NaOH. Micropor Mesopor Mater 2007;101:419–31.
[22] Torné-Fernández V, Mateo-Sanz J, Montané D, Fierro V. Statistical optimization of the synthesis of highly microporous carbons by chemical activation of Kraft lignin with NaOH. J Chem Eng Data 2009;54:2216–21.
[23] Fierro V, Torné-Fernández V, Celzard A, Montane D. Influence of the demineralisation on the chemical activation of Kraft lignin with orthophosphoric acid. J Hazard Mater 2007;149:126–33.
[24] Rodríguez-Mirasol J, Bedia J, Cordero T, Rodríguez J. Influence of water vapor on the adsorption of VOCs on lignin-based activated carbons. Sep Sci Technol 2005;40(15):3113–35.
[25] Silvestre-Albero A, Ramos-Fernández J, Martínez-Escandell M, Sepulveda-Escribano A, Silvestre-Albero J, Rodríguez-Reinoso F. High saturation capacity of activated carbons prepared from mesophase pitch in the removal of volatile organic compounds. Carbon 2010;48(2):548–56.
[26] Carrott PJM, Mourão PAM, Ribeiro Carrott MML, Gonçalves EM. Separating surface and solvent effects and the notion of critical adsorption energy in the adsorption of phenolic compounds by activated carbons. Langmuir 2005;21(25):11863–9.
[27] Mourão PAM, Carrott PJM, Ribeiro Carrott MML. Application of different equations to adsorption isotherms of phenolic compounds on activated carbons prepared from cork. Carbon 2006;44:2422–9.
[28] Seaton N, Walton J, Quirke N. A new analysis method for the determination of the pore size distribution of porous carbons from nitrogen adsorption measurements. Carbon 1989;27(6):853–61.
[29] Lastoskie C, Gubbins KE, Quirke N. Pore size distribution analysis of microporous carbons: a density functional theory approach. J Phys Chem 1993;97:4786–96.
[30] Do DD, Nicholson D, Do HD. Adsorption in micropores (nanopores): a computer appraisal of the Dubinin equations. Mol Simulat 2009;35(1–2):122–37.
[31] Ohba T, Kaneko K. GCMC study on relationship between DR plot and micropore width distribution of carbon. Langmuir 2001;17:3666–70.
[32] Ohba T, Suzuki T, Kaneko K. Relationship between DR-plot and micropore width distribution from GCMC simulation. Carbon 2000;38:1892–6.
[33] Neimark AV, Ravikovitch PI, Vishnyakov A. Bridging scales from molecular simulations to classical thermodynamics: density functional theory of capillary condensation in nanopores. J Phys Condens Matter 2003;15:347–65.
[34] Rege SU, Yang RT. Models for the pore-size distribution of microporous materials from a single adsorption isotherm. In: Tóth J, editor. Adsorption: theory, modeling, and analysis. New York: Marcel Dekker; 2002. p. 175–210.
[35] Neimark AV, Yangzheng L, Ravikovitch PI, Thommes M. Quenched solid density functional theory and pore size analysis of micro-mesoporous carbons. Carbon 2009;47:1617–28.
[36] Jagiello J, Olivier JP. A simple two-dimensional NLDFT model of gas adsorption in finite carbon pores. Application to pore structure analysis. J Phys Chem C 2009;113:19382–5.
[37] Do DD, Do HD. Modeling of adsorption on nongraphitized carbon surface. GCMC simulation studies and comparison with experimental data. J Phys Chem B 2006;110:17531–8.
[38] Yin YF, McEnaney B, Mays TJ. Dependence of GCEMC simulations of nitrogen adsorption on activated carbons on input parameters. Carbon 1998;36:1425–32.
[39] Bhatia SK. Density functional theory analysis of the influence of pore wall heterogeneity on adsorption in carbons. Langmuir 2002;18:6845–56.
[40] Nguyen TX, Bhatia SK. Characterization of activated carbon fibers using argon adsorption. Carbon 2005;43:775–85.
[41] Bandosz TJ, Biggs MJ, Gubbins KE, Hattori Y, Iiyama T, Kaneko K, et al. Molecular models of porous carbons. Chem Phys Carbon 2003;28:41–228.
[42] Ustinov EA, Do DD, Fenelonov VB. Pore size distribution analysis of activated carbons: application of density functional theory using nongraphitized carbon black as a reference system. Carbon 2006;44:653–63.
[43] Ravikovitch PI, Neimark AV. Density functional theory model of adsorption on amorphous and microporous silica materials. Langmuir 2006;22:11171–9.
[44] Carrott PJM, Marques LM, Carrott MMLR. Characterisation of the porosity of polymer and carbon aerogels containing Fe, Ni or Cu prepared from 2,4-dihydroxybenzoic acid by n-nonane pre-adsorption and density functional theory. Micropor Mesopor Mater 2010;131(1–3):75–81.
[45] Carrott PJM, Ribeiro Carrott MML, Roberts RA. Physical adsorption of gases by microporous carbons. Coll Surf 1991;58(4):385–400.
[46] Stoeckli HF, Rebstein P, Ballerini L. On the assessment of microporosity in active carbons, a comparison of theoretical and experimental data. Carbon 1990;28(6):907–9.
[47] Wood GO. Affinity coefficients of the Polanyi/Dubinin adsorption isotherm equations: a review with compilations and correlations. Carbon 2001;39:343–56.
[48] Hugi-Cleary D, Stoeckli F. On the use of standard DRK isotherms in Dubinin's t/F method. Carbon 2000;38:1309–13.
[49] Carrott PJM, Conceição FL, Ribeiro Carrott MML. Use of n-nonane pre-adsorption for the determination of micropore volume of activated carbon aerogels. Carbon 2007;45:1310–3.
[50] Carrott PJM, Cansado IPP, Carrott MMLR. On the L_o/σ ratio of the TVFM. Adsorpt Sci Technol 2006;24:205–13.
[51] Everett D, Powl J. Adsorption in slit-like and cylindrical micropores in Henrys law region – model for microporosity of carbons. J Chem Soc Faraday Trans I 1976;72:619–36.
[52] Setoyama N, Kaneko K, Rodríguez-Reinoso F. Ultramicropore characterization of microporous carbons by low-temperature helium adsorption. J Phys Chem 1996;100(24):10331–6.
[53] Sing KSW, Everett DH, Haul RAW, Moscou L, Pierotti RA, Rouquérol J, et al. Reporting physisorption data for gas/solid systems with special reference to the determination of surface area and porosity. Pure Appl Chem 1985;57:603–19.
[54] Kuwabara H, Suzuki T, Kaneko K. Ultramicropores in microporous carbon-fibers evidenced by helium adsorption at 4.2 K. J Chem Soc Faraday Trans 1991;87(12):1915–6.
[55] Mangun CL, Daley MA, Braatz RD, Economy J. Effect of pore size on adsorption of hydrocarbons in phenolic-based activated carbon fibers. Carbon 1998;36:123–9.
[56] Stoeckli F, Centeno TA, Fuertes AB, Muñiz J. Porous structure of polyarylamide-based activated carbon fibres. Carbon 1996;34:1201–6.